

# LatentArtiFusion: An Effective and Efficient Histological Artifacts Restoration Framework

Zhenqi He\*, Wenrui Liu\*, Minghao Yin, and Kai Han<sup>(✉)</sup>

The University of Hong Kong  
kaihanx@hku.hk

**Abstract.** Histological artifacts pose challenges for both pathologists and Computer-Aided Diagnosis (CAD) systems, leading to errors in analysis. Current approaches for histological artifact restoration, based on Generative Adversarial Networks (GANs) and pixel-level Diffusion Models, suffer from performance limitations and computational inefficiencies. In this paper, we propose a novel framework, LatentArtiFusion, which leverages the latent diffusion model (LDM) to reconstruct histological artifacts with high performance and computational efficiency. Unlike traditional pixel-level diffusion frameworks, LatentArtiFusion executes the restoration process in a lower-dimensional latent space, significantly improving computational efficiency. Moreover, we introduce a novel regional artifact reconstruction algorithm in latent space to prevent mistransfer in non-artifact regions, distinguishing our approach from GAN-based methods. Through extensive experiments on real-world histology datasets, LatentArtiFusion demonstrates remarkable speed, outperforming state-of-the-art pixel-level diffusion frameworks by more than 30×. It also consistently surpasses GAN-based methods by at least 5% across multiple evaluation metrics. Furthermore, we evaluate the effectiveness of our proposed framework in downstream tissue classification tasks, showcasing its practical utility. Code is available at <https://github.com/bugs-creator/LatentArtiFusion>.

**Keywords:** Histological Artifact Restoration · Diffusion Model

## 1 Introduction

Histological Whole Slide Images (WSI) provide ample information on tissue and nuclei structures, serving as a valuable resource for contemporary clinical diagnosis and informing treatment decisions [5,9]. Both pathologists and Computer-Aided Diagnosis (CAD) rely on the analysis of morphological and contextual information present in histological images. Nevertheless, the intricate digitization process and potential mishandling can commonly lead to alterations in tissue structure or staining information, such as tissue folding, bubbles, tissue mask, and other deformation [18,1,21]. Such deformation of tissue structures,

---

\* Equal contribution. The order is random.

namely artifacts in the context of pathology, not only poses challenges for both pathologists and Computer-Aided Diagnosis but also elevates the risk of misdiagnosis, *i.e.*, incorrectly identifying artifacts as tumors [25]. Many existing methods struggle to achieve satisfactory results in the presence of histological artifacts [28].

To address the challenge posed by the histological artifacts, many methods have been proposed based on Generative Adversarial Networks (GANs). For example, AR-CycleGAN [11] employs a Cycle Generative Adversarial Network (CycleGAN) [29,4] to learn the transfer between unpaired artifact and artifact-free images through adversarial learning. This model frames artifact restoration as a domain transfer problem, aiming to transform artifact images into clean images. However, this approach introduces a potential challenge of unintended stain style transfer in non-artifact regions, thereby increasing the risk of misdiagnosis. Additionally, GAN-based models are prone to failures during training due to mode collapse and mode dropping [2], posing challenges for their practical use. Recently, with the success of diffusion models [10,19], ArtiFusion [8] is introduced, which leverages the denoising diffusion probabilistic model [10] to selectively reconstruct the artifact region, aiming to preserve the structural and stain information of non-artifact areas. Further, a lightweight transformer based denoising backbone is employed for efficient histological artifact restoration [24]. While, the restorations is still taken by the denoising process of DDPM within the pixel-level space, which, given its substantial size, results in considerable computational costs. For example, DDPM based methods take approximately 30 times longer processing time compared to GAN-based methods, making it inefficient for real applications.

In this paper, we aim to achieve high performance on histological artifacts restoration while maintaining high computational efficiency. To this end, we propose **LatentArtiFusion**, in which we seamlessly integrate Variational AutoEncoder (VAE) [13] and the Denoising Diffusion Probabilistic Model (DDPM) [10]. This combination enables a denoising process within a perceptually equivalent space with lower-dimensions, thereby preserving the high performance of DDPM and achieving comparably lower computational costs. Moreover, a latent regional denoising process is proposed to simultaneously leverage and preserve the semantic information of adjacent non-artifact regions, specifically tailored for artifact restoration.

Our major contributions are: (1) We present a framework for histological artifact restoration, as the first attempt at latent diffusion models driven framework for histological artifact restoration. This approach opens up new possibilities for artifact restoration in histopathology. (2) We propose a novel regional latent denoising algorithm guided by artifact masks, allowing selective reconstruction of the artifact regions. This algorithm effectively preserves the stain style of non-artifact regions, resulting in visually consistent and coherent restorations. (3) Our method demonstrates superior efficiency, significantly surpassing previous pixel-level diffusion frameworks (*e.g.*, by over 30 times faster compared with ArtiFusion) in processing speed. Additionally, we achieve state-of-the-art results

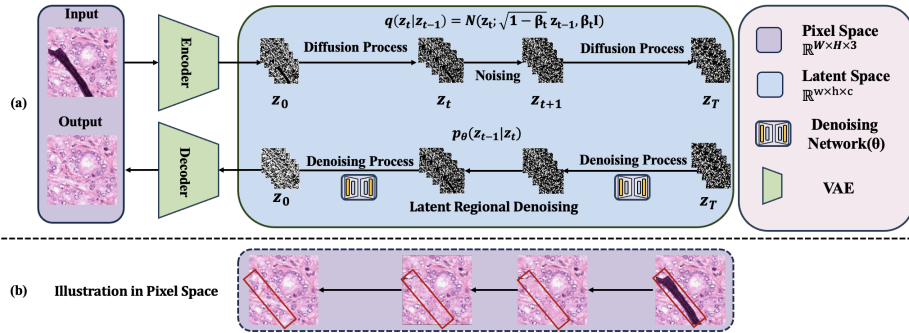


**Fig. 1.** (a) Overall architecture of the proposed **LatentArtiFusion** framework. (b) Visualization of latent regional denoising process in pixel-level space (Artifact region is marked with  $\square$ ).

across multiple datasets, highlighting the superior performance and effectiveness of our approach.

## 2 Method

### 2.1 Preliminary in Diffusion Models

**Denoising Diffusion Probabilistic Model (DDPM) [10].** DDPM learns the complex data distribution through diffusion and denoising process. In diffusion process, given the input data  $X_0 \sim p(X)$ , random Gaussian noise is gradually added into  $X_0$  to obtain the noisy version  $X_t$  for timestep  $t \in \mathbb{N}[0, T]$  following the Markov process  $q(\mathbf{x}_t|\mathbf{x}_{t-1}) = \mathcal{N}(\mathbf{x}_t; \sqrt{1 - \beta_t} \mathbf{x}_{t-1}, \beta_t \mathbf{I})$ , where  $T$  is the total diffusion timesteps,  $X_T \sim N(0, \mathbf{I})$  represents white noise without any semantic information, and  $\beta_t$  is the hyper-parameter representing the variance schedule. In the denoising process, a U-shaped denoising network with parameter  $\theta$  is trained to reverse the diffusion process  $q(\mathbf{x}_t|\mathbf{x}_{t-1})$  to learn  $p_\theta(\mathbf{x}_{t-1}|\mathbf{x}_t^{in})$  and gently denoise  $X_T$  back to  $X_0$  to recover the information of data  $X_0$ . The overall training objectives are formulated by the variational lower bound of the negative log-likelihood and can be written as:

$$L = \mathbb{E}_q \left[ \underbrace{D_{KL}(q(\mathbf{x}_T|x_0))}_{L_T} \right] + \sum_{t>1} \left[ \underbrace{D_{KL}(q(\mathbf{x}_{t-1}|\mathbf{x}_t, \mathbf{x}_0))}_{L_{t-1}} \right] - \underbrace{\log p_\theta(\mathbf{x}_0|\mathbf{x}_1)}_{L_0},$$

where  $D_{KL}(\cdot||\cdot)$  is the KL divergence.

**Latent Diffusion Models (LDM) [17].** Denoising in large data space, *i.e.*, pixel-level space  $\mathbb{R}^{W \times H \times 3}$ , is relatively computationally costly and inefficient. To reduce the computational costs, LDM conducts the diffusion and denoising

process in a lower-dimensional latent space through compressing data  $X$  through Variational Auto-Encoder  $\varepsilon(\cdot)$  (VAE) [13] structure into a smaller dimensional space  $\mathbb{R}^{w \times h \times c}$ , and output the decoded  $\hat{X} = D(\varepsilon(X))$ , where  $\varepsilon$  and  $D$  are the encoder and decoder of the VAE.

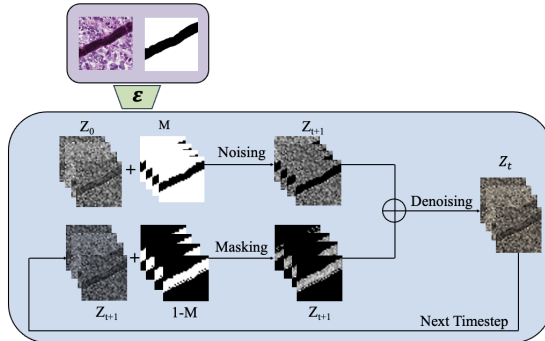


**Fig. 2.** Regional denoising in latent space to selectively denoising the artifact regions while preserving the clean regions.

## 2.2 LatentArtiFusion

**Overall Pipeline.** The comprehensive architecture of our proposed framework is illustrated in Fig. 1(a). The framework comprises two key stages: training and inference, constituting the backbone of our restoration approach. During the training stage, our primary objectives involve the training of a latent diffusion model. This model assimilates contextual information and captures the color distribution inherent in real artifact-free histology images. In the inference stage, We propose a novel latent regional denoising algorithm to selectively reconstruct artifact regions in latent space leveraging the semantic information of nearby artifact-free regions to preserve the morphological details of non-artifact regions and maintain visual consistence in reconstructed artifact regions. Fig. 1(b) visually represents the latent regional denoising process in pixel-level space to demonstrate the gradual reconstruction of the artifact region.

**Model Training.** For efficiency, we follow the formulation of the latent diffusion model to train our model from scratch in a lower-dimensional latent space. Initially, we utilize a pre-trained Variational Autoencoder (VAE) [13] to compress the input image  $X \in \mathbb{R}^{W \times H \times 3}$  into the latent space  $\mathbb{R}^{w \times h \times c}$ . Subsequently, we perform the diffusion and denoising processes within this latent space, aiming to enhance computational efficiency. Given a compressed image  $Z_0 = \varepsilon(X) \in \mathbb{R}^{w \times h \times c}$ , random Gaussian noises are gradually injected following the Markov Chain  $q(\mathbf{z}_t | \mathbf{z}_{t-1}) = \mathcal{N}(\mathbf{z}_t; \sqrt{1 - \beta_t} \mathbf{z}_{t-1}, \beta_t \mathbf{I})$ , as shown in Fig. 1 (a).

Subsequently, we train a U-shaped denoising network, which takes  $\mathbf{z}_t$  conditioned on the time  $t$  as input, to predict the corresponding noise added from  $\mathbf{z}_{t-1}$  to  $\mathbf{z}_t$  in the denoising process. This allows us to learn  $p_\theta(\mathbf{z}_{t-1}|\mathbf{z}_t)$  and sample the noisy data back to input data  $\mathbf{z}_0$  step by step.

Crucially, we utilize the pre-trained VAE<sup>1</sup> by [17], and all parameters of the VAE are frozen throughout the model training process.

**Regional Denoising in Latent Space.** During the inference stage, we introduce an innovative latent regional denoising algorithm. This algorithm selectively focuses on reconstructing the artifact region in the latent space, deviating from the conventional approach of reconstructing the entire image. As shown in Fig. 2, the compressed histology image with artifacts and its corresponding artifact mask in the latent space retain the semantic information of artifacts, we leverage the compressed mask to precisely guide the restoration process, focusing exclusively on the artifact regions. To perform regional denoising in the artifact region while preserving non-artifact regions in the latent space, we encode the Boolean mask representing the localization of the artifact region into the latent space (denoted as  $M$ ). At each denoising timestep  $t$ , the input to the denoising network ( $\theta$ ) is a concatenation of the noised non-artifact regions (occurring  $t$  times) with the denoised artifact region obtained from the denoising network at the previous step ( $t + 1$ ). The whole latent regional denoising process can be formulated as follows:

$$\begin{aligned} \mathbf{Z}_t &= \text{Denoising}[\mathbf{Z}_{t+1}^{sample} \odot \mathbf{M} + \mathbf{Z}_{t+1}^{output} \odot (1 - \mathbf{M})], \\ \mathbf{Z}_{t+1}^{sample} &= \sqrt{\bar{a}_t} \mathbf{Z}_0 + \sqrt{1 - \bar{a}_t} \epsilon_t, \end{aligned} \quad (1)$$

where  $\mathbf{Z}_t^{sample} \odot \mathbf{M}$  is non-artifact region diffused as  $t$  times from the compressed input data  $Z_0$ , following the forward Gaussian process with  $\bar{a}_t = \prod_{i=1}^t (1 - \beta_i)$ . Additionally,  $\mathbf{Z}_{t+1}^{output}$  denotes the output of the denoising network at previous timestep *i.e.*,  $p_\theta(\mathbf{z}_{t+1}^{output}|\mathbf{z}_{t+2})$ , and the  $\mathbf{Z}_t$  is used as  $\mathbf{Z}_t^{output}$  in subsequent time step. Through iteration, the reconstructed sample can be obtained as  $\hat{\mathbf{Z}}_0 = \text{Denoising}[\mathbf{Z}_1^{sample} \odot \mathbf{M} + \mathbf{Z}_1^{output} \odot (1 - \mathbf{M})]$ .

## 3 Experiments

### 3.1 Implementation details

We implement the proposed LatentArtiFusion in Python 3.10 and PyTorch 2.1 with Diffusers [16]. Hyperparameters are set as follows: batch size is 16, learning rate is  $1 \times 10^{-4}$  with the Adam optimizer, the downsample factor of the VAE is set to 8, linear variance scheduler is used, and the number of total timesteps is set to 50.

<sup>1</sup> Pretrained weights are downloaded from <https://huggingface.co/runwayml/stable-diffusion-v1-5>.

**Table 1.** Quantitative comparison of the proposed method with CycleGAN and ArtiFusion [8] on artifact restoration performance in terms of the similarities between original images and restored images. The best performance for each indicator is highlighted in **boldface**.  $\downarrow$  denotes lower is better;  $\uparrow$  denotes higher is better.

Dataset	Methods	L2 ( $\times 10^4$ ) $\downarrow$	MSE $\downarrow$	SSIM $\uparrow$	PSNR $\uparrow$	FSIM $\uparrow$
Histology	CycleGAN [29]	1.8930	0.5936	0.9622	42.12	0.7162
	ArtiFusion [8]	0.4940	0.2465	<b>0.9860</b>	<b>48.08</b>	0.8216
	<b>Ours</b>	<b>0.4493</b>	<b>0.2320</b>	0.9810	46.92	<b>0.8913</b>
MoNuSAC2020	CycleGAN [29]	13.81	7.250	0.8876	40.04	0.7094
	ArtiFusion [8]	4.034	2.117	0.9325	40.16	0.7412
	<b>Ours</b>	<b>3.930</b>	<b>2.063</b>	<b>0.9505</b>	<b>42.01</b>	<b>0.8752</b>

**Table 2.** Comparison of model efficiency in terms of (1) the averaged inference time for each image with the size of  $256 \times 256 \times 3$  and (2) the number of required steps for the diffusion process (Not applicable for CycleGAN).

Methods	Inference(s)	Diffusion steps
CycleGAN [29]	1.065	<i>N/A</i>
ArtiFusion [8]	30.71	250
<b>Ours</b>	<b>0.8341</b>	<b>50</b>

### 3.2 Datasets

We use a subset of Camelyon17 [14] comprised of 2445 artifact-free images with the resolution of  $256 \times 256$  as the training set <sup>2</sup>. To evaluate the performance and robustness of our model, we test on two different data sources containing multiple cell types. (1) Histology: a public histology dataset <sup>3</sup>, which is widely used for nuclei segmentation task [12,9], consists of 462 artifact-free images collected from multiple patients with densely clustered nuclei. (2) MoNuSAC 2020 [22]: another public dataset of 154 artifact-free tissue images scanned from various organs. In the two test sets, we manually synthesize artifacts into original artifact-free images to obtain paired artifact and artifact-free images for performance evaluation.

### 3.3 Comparison and Results

To quantitatively analyze the restoration performance and computational efficiency, we measure the similarities between unprocessed clean images and restored artifact images using the following evaluation metrics,  $L_2$  distance ( $L_2$ ) over the whole image, the mean-squared error (MSE) specifically focused on the artifact region, structural similarity index (SSIM) [26], peak signal-to-noise ratio (PSNR) [3] and feature-based similarity index (FSIM) [27]. Additionally, we

<sup>2</sup> Available at <https://github.com/zhenqi-he/ArtiFusion>.

<sup>3</sup> Available at <https://github.com/zhenqi-he/transnuseg>.

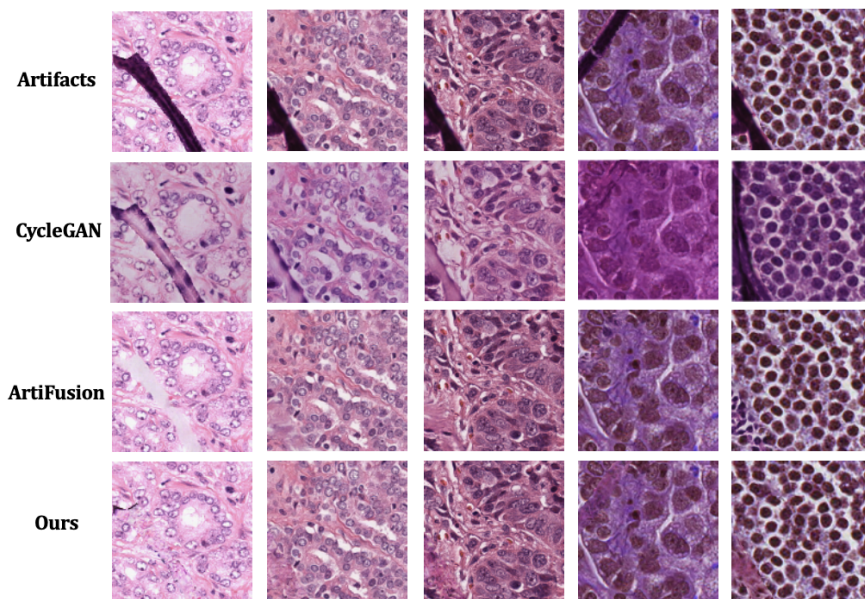


**Fig. 3.** Qualitative comparison of the restoration by CycleGAN [29], pixel-level ArtiFusion [8], and **Ours**. The first three images are selected from Histology Dataset [9] and the last two are from MoNuSAC2020 [22].

measure the time costs during inference. We compare our model with the state-of-the-art models, CycleGAN [29] and ArtiFusion [8]. The quantitative comparisons are shown in Table 1 and Table 2. Visualized results are demonstrated in Fig. 3.

Quantitative comparisons across two distinct data sources highlight the success of our proposed framework in effectively reconstructing tissue structures within artifact regions while maintaining high computational efficiency. The substantial performance gaps observed across all evaluation metrics between CycleGAN [29] and our method corroborate that our latent regional denoising algorithm excels in selectively reconstructing the artifact region while successfully preserving both color and structural information in non-artifact regions. In contrast to the previous pixel-level approach of ArtiFusion [8], denoising in the latent space accelerates the inference time by more than 30 times, resulting in a substantial reduction from 30 seconds to just 0.8 seconds. Moreover, fewer reconstruction steps are required, leading to significant savings in computational resources.

Overall, our method outperforms the other methods in all metrics across different datasets of various nuclei types collected from multiple organs. At the same time, our method obtains a significant increase by  $30\times$  and  $1.2\times$  respectively in the inference time compared with ArtiFusion [8] and CyclyGAN [29].

**Table 3.** Quantitative comparison in the downstream tissue classification task. ‘Clean’ indicates unprocessed original images, ‘Artifacts’ means synthetic artifact images, and ‘Restored w [MODEL]’ indicates that the images are restored by the corresponding model. We evaluate the classification accuracy (%) on the test set with different network architectures including ResNet [7], ConvNeXt [15], CSPNet [23], RexNet [6] and EfficientNet [20].

Settings	ResNet18	ConvNeXt_small	CSPDarkNet53	RexNet100	EfficientNetB0
Clean	95.529	95.738	94.382	95.487	95.808
Artifacts	80.302	86.533	82.210	90.446	90.626
Restored w CycleGAN	86.326	87.201	86.429	90.776	91.811
Restored w ArtiFusion	92.376	91.416	89.792	92.310	94.232
Restored w <b>Ours</b>	<b>93.201</b>	<b>93.042</b>	<b>91.117</b>	<b>93.001</b>	<b>94.694</b>

Moreover, our proposed LatentArtiFusion achieves 80% computational reduction in the reconstruction stage.

### 3.4 Downstream Classification Evaluation

To validate the effectiveness of our framework in reducing the misdiagnosis rate, we further conduct a downstream classification task. We utilize the publicly available NCT-CRC-HE-100K tissue classification dataset for training and the CRC-VAL-HE-7K dataset for testing. The training set comprises a total of 100,000 samples, while the test set consists of 7,180 samples. Various classification models are employed to ensure the robustness of the evaluation across different model architectures. After training all classification models on the training set, we assess their performance on the test data under three different conditions: (a) clean images, (b) images with synthetic artifacts, and (c) artifact images restored by a specific method. Note that the classification result on clean images serves as the upper bound, while the test result on artifact images represents the lower bound. The quantitative results are shown in Table 3.

A substantial decrease of up to 15% in the classification results across all models is observed when comparing unprocessed data to data with artifacts, demonstrating the disruptive impact of artifacts on deep-learning approaches. The considerable performance gap between CycleGAN [29] and diffusion-based methods further validates the superiority of the denoising diffusion model in histological artifact restoration. Crucially, artifact images restored by our method exhibit the highest classification performance across various model architectures when compared with artifact images reconstructed by CycleGAN [29] and ArtiFusion [8]. Through restoration by our framework, the classification accuracy is improved from approximately 80% to a remarkable 93%, which is very close to the classification result using clean images. This underscores the practical effectiveness of our framework in downstream tasks.



## 4 Conclusion

In this paper, we have presented an efficient and effective framework, LatentArtiFusion, for histological artifact restoration, which subtly integrates VAE and DDPM, resulting in a strong model for artifact restoration in a lower-dimensional latent space, leading to a significant increase in computational efficiency. Further, we have introduced a regional denoising algorithm in the latent space that successfully preserves the tissue and nuclei information of non-artifact regions. The experimental results demonstrate the superiority of our method over previous works across multiple datasets.

**Disclosure of Interests.** The authors have no competing interests to declare that are relevant to the content of this article.

## References

1. Babu, N.A., Anjuga, E.S., Masthan, K., Rajesh, E.: Artifacts in histopathology—a review. *Indian Journal of Forensic Medicine and Toxicology* (2020)
2. Creswell, A., White, T., Dumoulin, V., Arulkumaran, K., Sengupta, B., Bharath, A.A.: Generative adversarial networks: An overview. *IEEE Signal Processing Magazine* (2018)
3. Faragallah, O.S., El-Hoseny, H., El-Shafai, W., El-Rahman, W.A., El-Sayed, H.S., El-Rabaie, E.S.M., El-Samie, F.E.A., Geweid, G.G.N.: A comprehensive survey analysis for present solutions of medical image fusion and future directions. *IEEE Access* (2021)
4. Goodfellow, I., Pouget-Abadie, J., Mirza, M., Xu, B., Warde-Farley, D., Ozair, S., Courville, A., Bengio, Y.: Generative adversarial networks. *Communications of the ACM* (2020)
5. Gurcan, M.N., Boucheron, L.E., Can, A., Madabhushi, A., Rajpoot, N.M., Yener, B.: Histopathological image analysis: A review. *IEEE Reviews in Biomedical Engineering* (2009)
6. Han, D., Yun, S., Heo, B., Yoo, Y.: Rexnet: Diminishing representational bottleneck on convolutional neural network. In: *CVPR* (2021)
7. He, K., Zhang, X., Ren, S., Sun, J.: Deep residual learning for image recognition. In: *CVPR* (2016)
8. He, Z., He, J., Ye, J., Shen, Y.: Artifact restoration in histology images with diffusion probabilistic models. In: *MICCAI* (2023)
9. He, Z., Unberath, M., Ke, J., Shen, Y.: Transnuseg: A lightweight multi-task transformer for nuclei segmentation. In: *MICCAI* (2023)
10. Ho, J., Jain, A., Abbeel, P.: Denoising diffusion probabilistic models. In: *CoRR* (2020)
11. Ke, J., Liu, K., Sun, Y., Xue, Y., Huang, J., Lu, Y., Dai, J., Chen, Y., Han, X., Shen, Y., Shen, D.: Artifact detection and restoration in histology images with stain-style and structural preservation. *IEEE TMI* (2023)
12. Ke, J., Lu, Y., Shen, Y., Zhu, J., Zhou, Y., Huang, J., Yao, J., Liang, X., Guo, Y., Wei, Z., Liu, S., Huang, Q., Jiang, F., Shen, D.: Clusterseg: A crowd cluster pinpointed nucleus segmentation framework with cross-modality datasets. *MIA* (2023)

13. Kingma, D.P., Welling, M.: An introduction to variational autoencoders. *Foundations and Trends in Machine Learning* (2019)
14. Litjens, G., Bandi, P., Ehteshami Bejnordi, B., Geessink, O., Balkenhol, M., Bult, P., Halilovic, A., Hermsen, M., van de Loo, R., Vogels, R., et al.: 1399 h&e-stained sentinel lymph node sections of breast cancer patients: the camelyon dataset. *GigaScience* (2018)
15. Liu, Z., Mao, H., Wu, C.Y., Feichtenhofer, C., Darrell, T., Xie, S.: A convnet for the 2020s. In: *CVPR* (2022)
16. von Platen, P., Patil, S., Lozhkov, A., Cuenca, P., Lambert, N., Rasul, K., Davaadorj, M., Nair, D., Paul, S., Berman, W., Xu, Y., Liu, S., Wolf, T.: Diffusers: State-of-the-art diffusion models. <https://github.com/huggingface/diffusers> (2022)
17. Rombach, R., Blattmann, A., Lorenz, D., Esser, P., Ommer, B.: High-resolution image synthesis with latent diffusion models. In: *CVPR* (2022)
18. Seoane, J., Varela-Centelles, P., Ramírez, J., Cameselle-Teijeiro, J., Romero, M.: Artefacts in oral incisional biopsies in general dental practice: a pathology audit. *Oral diseases* (2004)
19. Song, Y., Sohl-Dickstein, J., Kingma, D.P., Kumar, A., Ermon, S., Poole, B.: Score-based generative modeling through stochastic differential equations. In: *ICLR* (2021)
20. Tan, M., Le, Q.V.: Efficientnet: Rethinking model scaling for convolutional neural networks. In: *ICML* (2020)
21. Taqi, S.A., Sami, S.A., Sami, L.B., Zaki, S.A.: A review of artifacts in histopathology. *Journal of oral and maxillofacial pathology: JOMFP* (2018)
22. Verma, R., etc.: Monusac2020: A multi-organ nuclei segmentation and classification challenge. *IEEE TMI* (2021)
23. Wang, C.Y., Mark Liao, H.Y., Wu, Y.H., Chen, P.Y., Hsieh, J.W., Yeh, I.H.: Cspnet: A new backbone that can enhance learning capability of cnn. In: *CVPR Workshops* (2020)
24. Wang, C., He, Z., He, J., Ye, J., Shen, Y.: Histology image artifact restoration with lightweight transformer based diffusion model. In: *Artificial Intelligence in Medicine - AIME* (2024)
25. Wang, N.C., Kaplan, J., Lee, J., Hodgins, J., Udager, A., Rao, A.: Stress testing pathology models with generated artifacts. *Journal of Pathology Informatics* (2021)
26. Wang, Z., Bovik, A., Sheikh, H., Simoncelli, E.: Image quality assessment: from error visibility to structural similarity. *IEEE TIP* (2004)
27. Zhang, L., Zhang, L., Mou, X., Zhang, D.: Fsim: A feature similarity index for image quality assessment. *IEEE TIP* (2011)
28. Zhang, Y., Sun, Y., Li, H., Zheng, S., Zhu, C., Yang, L.: Benchmarking the robustness of deep neural networks to common corruptions in digital pathology. In: *MICCAI* (2022)
29. Zhu, J.Y., Park, T., Isola, P., Efros, A.A.: Unpaired image-to-image translation using cycle-consistent adversarial networks. In: *ICCV* (2017)